Empa
Materials Science and Technology

ETH zürich

Semester Project

Cyclic plasticity and fatigue response of SLM Hastelloy X at 700°C

Mathias Kuhlow

June 2021

Advisors:

Prof. Dr. E. Mazza, Dr. E. Hosseini

Institute of Mechanical Systems, ETH Zürich
Experimental Continuum Mechanics, Empa

Abstract

Additive manufacturing of high temperature alloys has been recently attracted a vast amount of interest, as the technology enables fabricating components with functionally optimized designs and complex geometries. Despite this importance, very limited information exists in literature about the mechanical response of such AM alloys at elevated temperature. This study is about the investigation of the cyclic plasticity and fatigue response of AM Hastelloy X at 700°C. 17 strain-controlled fatigue tests were performed for samples with two different conditions: as-built and surface machined. The results obtained from these tests were then compared with other reports for AM-Hastelloy X at other temperatures or conventionally fabricated Hastelloy X.

Results from the fatigue tests have shown that there are big differences in the fatigue life of a test specimen, depending on its surface condition, temperature, applied strain amplitude or manufacturing method. LPBF-Hastelloy X can show both, cyclic hardening or cyclic softening. Serrated flow behaviour can be observed in stress-strain hystereses. A large scatter in the results was noticed and can be explained by internal porosities or defects on the surface caused by the additive manufacturing process.

Acknowledgment

First of all, I want to thank Prof. Dr. Edoardo Mazza for giving me the opportunity to do my semester project in the Experimental Continuum Mechanics laboratory at EMPA.

A special thank goes to Dr. Ehsan Hosseini, for supervising my project over past few months. With his huge knowledge he helped and supported me in many situations and he always took his time when needed. It was very pleasant to work with him.

Additionally I want to thank Dr. Valliappa Kalyanasundaram for his support and explanations about the testing procedure, Xiaolong Li for the continuation of the tests, Jian Tang for taking SEM-images for me and the whole team of the HTIG for an educational and pleasant stay at EMPA.

And last but no least I want to thank Reza Esmaeilizadeh from University of Waterloo for providing me his documents and always answering my questions.

Contents

Chapter 1

Introduction

1.1 Motivation

Hastelloy X, also known as HX alloy, which has been investigated during this project is a nickel-based solid solution strengthened superalloy. It is used in various components, such as gas turbine blades, tail pipes or combustor chambers. Hastelloy X is characterized by its excellent oxidation and nitriding resistance and good strength at high temperatures [1, 2, 3].

Additive manufacturing (AM) processes such as laser powder-bed fusion (LPBF) are rapidly advancing over the past years due to their many advantages compared to conventional manufacturing [4]. Beside of a tool-less production from "Lot Size One", the functional integration of other parts, lightweight design or the ability to produce very complex structures is possible [5]. An example for an application in the high-temperature sector, in which Hastelloy X is used, Magerramova et al. [6] demonstrated the possibility of using AM for the manufacture of turbine blades with embedded internal cooling channels, which cannot be manufactured by conventional methods.

Despite the many benefits of AM, there are still some challenges that need to be overcome. Metallic LPBF-parts present several defects in terms of pores and surface roughness, where these defects can drastically affect the material properties [7, 8]. Reliable mechanical properties of the manufactured AM-parts are a prerequisite for series production and thus a need to be more deeply investigated [7]. For load bearing parts, mechanical response of metallic AM-parts is according to Esmaeilizadeh [9] one of the main properties to study. Because of rapid solidification and high cooling rates during manufacturing LPBF-parts show a finer microstructure and therefore better properties under quasi-static conditions than conventional manufactured parts [10]. Apart from that, internal defects or the surface roughness of AM structures are a main

reason why they show a inferior fatigue behaviour than conventionally made parts [9]. There exist very few studies about the mechanical response of LPBF HX, especially for fatigue response. Therefore a more detailed examination of fatigue properties of HX at high temperature is necessary.

1.2 Objective of the Project

The aim of this project is to conduct fatigue tests at high temperatures to characterise the fatigue behaviour of LPBF-Hastelloy X. Esmaeilizadeh et al. [11] investigated in their recent study the effect of LPBF process parameters on the quasi-static and fatigue behaviour of Hastelloy X. Optimized process parameters were then used to manufacture the specimens used for this project. With the same specimens LCF-tests at room temperature were performed by Esmaeilizadeh [9]. For the high-temperature tests 700°C was chosen, because Saarimäki et al. [12] have done fatigue crack growth tests on AM HX at this temperature and claimed that this is the working temperature and the temperature at which the material's properties start to deteriorate.

Another aspect which is investigated in this project is the surface condition. As mentioned above, the surface roughness has a major influence on the fatigue life of a part. This investigation is important, because AM is often used for complex geometries where a post-processing of the surface is challenging or impossible.

The results from the fatigue experiments were then compared with data from the literature. The following comparisons of the fatigue response are made:

- Room temperature LPBF-HX vs. LPBF-HX at 700°C
- Additive manufactured HX vs. conventional manufactured HX
- Effect of surface roughness: as-built vs. surface machined LBPF-HX

Chapter 2

Literature Review

2.1 Hastelloy X

The material used for this project is Hastelloy X (HX), a nickel-based solid solution strengthened superalloy. It's chemical composition is shown in table 2.1. The presence of the high percentage of Ni results in good strength even at higher temperatures while chromium is responsible for high oxidation resistance [13]. Hastelloy X has excellent forming and welding characteristics. It is widely used in high temperature applications like gas turbine burners, tail pipes, jet engines or combuster chambers [3, 12, 10]. Some typical properties of conventional manufactured HX are listed in table 2.2.

Table 2.1: Nominal chemical composition of Hastelloy X [13].

Element	Ni	Cr	Fe	Mo	Co	W	C	Mn	Si	B
Composition [%]	47[a]	22	18	9	1.5	0.6	0.1	1[b]	1[b]	0.008[b]

[a] As balance
[b] Maximum

Parts made of Hastelloy X manufactured in a LBFP-process as described in section 2.2 show different mechanical properties compared to conventional manufactured ones [10]. One reason for this is the ultrafine solidification microstrucutre caused by high cooling rates during additive manufacturing [9]. Wang [10] compared the mechanical properties of hot forged HX and SLM-HX. He showed that yield stress and ultimate tensile stress of SLM specimens are higher and the elongation is lower than the hot forged alloy. According to Saktihivel et al. [1] Hastelloy X shows a complicated yielding behaviour in the intermediate temperature range. This can be attributed to dynamic strain aging (DSA) behaviour, which is discussed in section 2.5. According to Miner and Castelli [2] conventional manufactured Hastellox X exhibits cyclic

hardening over a wide temperature range between about 200°C and 700°C. This phenomenon is described in more detail in section 2.4.

Table 2.2: Typical physical properties of conventionally manufactured Hastelloy X [13].

Density [kg/m^3]	**Melting range** [°C]	**Elastic modulus** [GPa]	**Yield stress** [MPa]
8220	1260 to 1355	205 (at 25°C)	380 (at 25°C)

2.2 Selective Laser Melting

Additive Manufacturing (AM) or 3D printing is a general expression for a process that builds object from three-dimensional digital models, usually by adding material layer-by-layer [14]. There exist many different system configurations for AM, based in various technologies. For Metal Additive Manufacturing (MAM) one of the most used technology is Selective Laser Melting (SLM), also referred to as Laser Powder Bed Fusion (LPBF) [15]. The general working principle of SLM is shown in figure 2.1. A laser beam is directed by a scanner system at a bed of powder to fuse a layer defined by the cross sectional area of the sliced 3D-model. The laser follows a predefined scan path of overlapping weld beads. After a layer is finished the powder bed and the part are then incrementally dropped and recoated by a roller or blade adding a new layer of powder. Then the next layer is melted selectively and solidified and fuses with the previous layer until the complete part is formed [16]. The process is influenced by a large number of different parameters, which makes an optimization for different materials necessary. Examples for process parameters are scanning speed, layer thickness, laser power or hatching distance between two paths [15]. To acknowledge, the main disadvantages of the SLM-technology are low production rate, the need of support structure or necessary post-processes as powder removal or heat treatment [17].

2.3 Fatigue

2.3.1 Theory of Fatigue

Fatigue is defined as a process of the cycle-by-cycle accumulation of damage in a material undergoing fluctuating stress and strains [18]. A main feature of fatigue is that the load is usually not large enough to cause immediate failure. Instead, failure occurs after a certain number of load cycles, i.e. after the

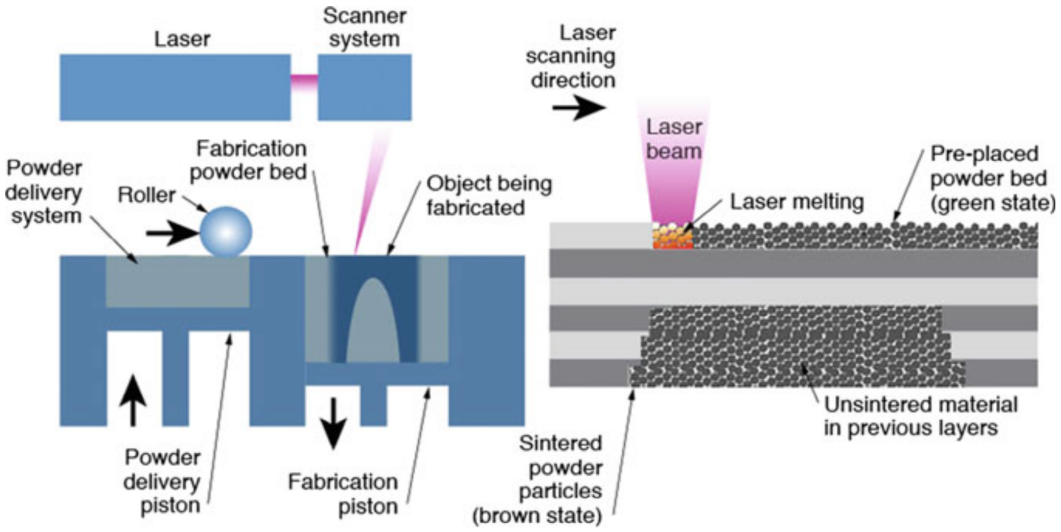

Figure 2.1: Selective Laser Melting (SLM) technology [15].

accumulated damage has reached a critical level. According to Cui [19] fatigue failure is one of the most common failure modes of metallic structures.
Fatigue crack formation and growth can be divided into three stages. A crack usually starts from the surface, where fatigue damage begins as shear cracks on slip planes (stage I). Then, after a transient period, crack growth occurs in a direction normal to the applied stress (stage II). Finally, fracture occurs after the crack becomes unstable (stage III). Figure 2.2 shows a schematic representation of these three stages [19].
According to Schijve [20] differentiating between the crack initiation period and the crack growth period is very important because several surface conditions do affect the initiation period, but have a negligible influence on the crack growth period. For predictions on crack initiation and crack growth, the important parameter is the stress concentration factor K_t and the stress intensity factor K respectively.
Crack initiation starts mostly at the material surface. A reason is the inhomogeneous stress distribution due to a notch effect of an unevenness or roughness. As a result a stress concentration occurs at the surface. Therefore Schijve summarizes:

"In the crack initiation period fatigue is a material surface phenomenon." [20]

This implies that the surface condition has a big influence on the crack nucleation and K_t is the dominating factor within the crack initiation period.
An existing microcrack contributes to an inhomogeneous stress distribution with a stress concentration at the tip of the crack. As a result, the crack starts growing into the material, in general with a tendency to grow perpendicular to

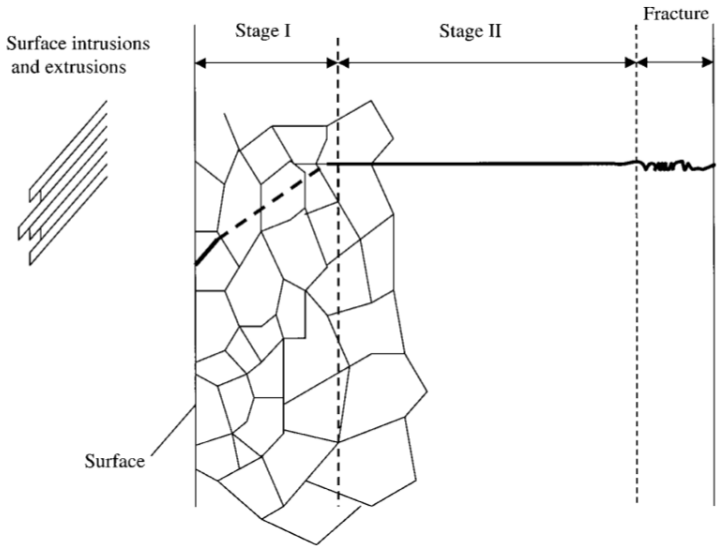

Figure 2.2: Schematic representation of fatigue crack formation and growth in metals [19].

the loading direction. The crack growth rate can vary during crack formation and depends for instance on the number of grain boundaries which function as a barrier for the crack. How fast a crack will grow depends on the crack growth resistance of the material. Thus the following holds:

"Crack growth resistance when the crack penetrates into the material depends on the material as a bulk property. Crack growth is no longer a surface phenomenon." [20]

2.3.2 Fatigue Life Modelling

Fatigue is the primary failure mechanism in most engineering components. Hence, the accurate prediction of the fatigue life is of critical importance. As described in section 2.3.1 fatigue damage increases with applied cycles in a cumulative manner, which can lead to fracture. Based on this consideration a way to predict the fatigue life of a material is the cumulative fatigue damage (CFD) theory [19]. In this section two different CFD-approaches to model the fatigue life are described: The Basquin-Coffin-Manson relationship [21, 22] and the Jahed-Varani relationship [23].

The strain-based Basquin-Coffin-Manson (BCM) equation is mostly used for modeling strain-life response of metals. The total strain applied during a cycle can be divided into an elastic and a plastic part. The elastic ($\varepsilon_{a,elastic}$) and

plastic ($\varepsilon_{a,plastic}$) strain amplitudes are defined by the Basquin and Coffin-Manson equations, respectively as:

$$\varepsilon_{a,elastic} = \frac{\sigma_f^{'}}{E}(2N_f)^b \tag{2.1}$$

$$\varepsilon_{a,plastic} = \varepsilon_f^{'}(2N_f)^c \tag{2.2}$$

where E is the modulus of elasticity and N_f are the cycles to failure. $\sigma_f^{'}$ and b are the fatigue strength coefficient and fatigue strength exponent, respectively, and $\varepsilon_f^{'}$ and c are fatigue ductility coefficient and fatigue ductility exponent, respectively [24].

The procedure to find the parameters for Eq. 2.1 and Eq. 2.2 can be found using the Standard Practice for Statistical Analysis of Linear or Linearized Stress-Life (S-N) and Strain-Life (ε-N) Fatigue Data [25]. Figure 2.4 (a) shows a schematic illustration of the elastic and plastic strain amplitudes obtained from the midlife hysteresis loop. The total strain amplitude, ε_a, is then obtained from the superposition of its elastic and plastic part by combining Eq. 2.1 and Eq. 2.2:

$$\varepsilon_a = \varepsilon_{a,elastic} + \varepsilon_{a,plastic} = \frac{\sigma_f^{'}}{E}(2N_f)^b + \varepsilon_f^{'}(2N_f)^c \tag{2.3}$$

Figure 2.3 shows an example of the representation of elastic, plastic, and total strain resistance to fatigue loading [19].

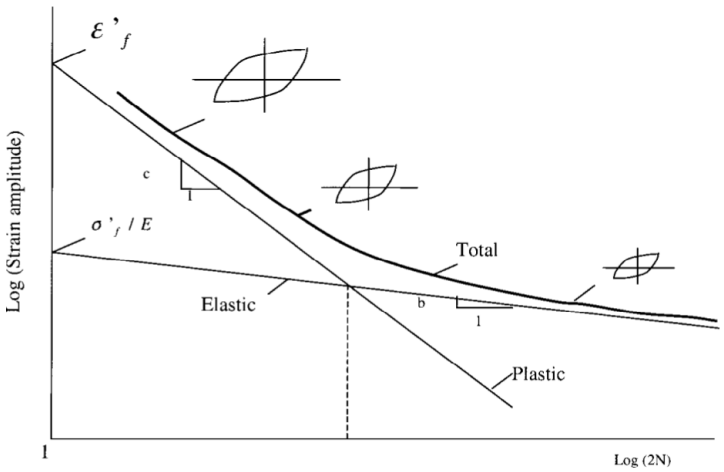

Figure 2.3: Representation of elastic, plastic, and total strain resistance to fatigue loading [19].

The energy-based Jahed-Varani (JV) equation is another approach to model the fatigue life, but instead of strain- it is energy-based. It assumes that the dissipated energy density during cyclic loading has a major contribution to the fatigue damage process, especially in the LCF regime [23]. Because energy is a scalar parameter, the strain energy corresponding to different stress/strain components can be manipulated algebraically, without the concern of different material orientation or loading direction [26]. Analogue to the BCM-model the total strain energy density consists of its elastic and plastic part. The positive elastic strain energy density, $\triangle E_e^+$, and the plastic strain energy density, $\triangle E_p$, can be obtained out of the midlife hysteresis loop. $\triangle E_e^+$ can be calculated by Eq. 2.4, where σ_{max} is the tensile peak stress and E the elastic modulus. $\triangle E_p$ is calculated from the area inside the midlife hysteresis loop by Eq. 2.5 [24].

$$\triangle E_e^+ = \frac{\sigma_{max}^2}{2E} \tag{2.4}$$

$$\triangle E_p = \oint \sigma \, d\varepsilon \tag{2.5}$$

Figure 2.4 (b) shows schematically the positive elastic and plastic strain energies in the midlife hysteresis loop. The total strain energy density $\triangle E$ is related to the fatigue reversals by:

$$\triangle E = \triangle E_e^+ + \triangle E_p = E_e^{'}(2N_f)^B + E_f^{'}(2N_f)^C \tag{2.6}$$

where $E_e^{'}$, B, $E_f^{'}$, C are the fatigue strength coefficient, the fatigue strength exponent, the fatigue toughness coefficient, and the fatigue toughness exponent, respectively [24].

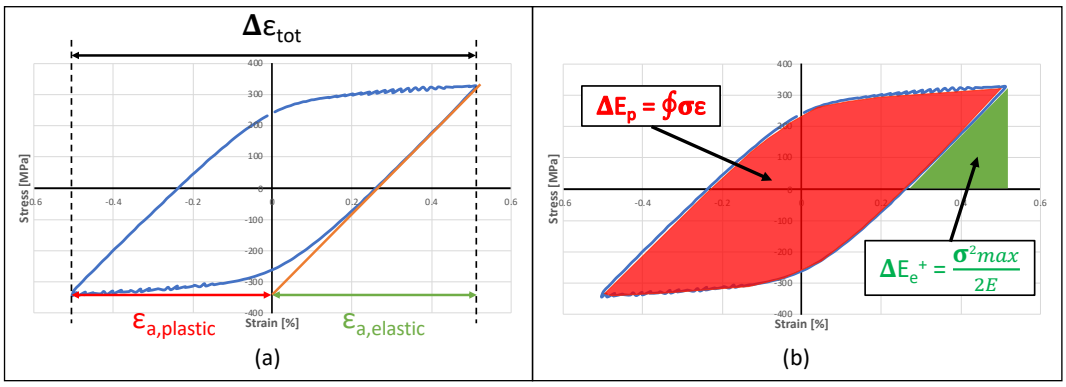

Figure 2.4: a) Schematic illustration of elastic and plastic strain ranges,
b) Schematic illustration of positive elastic and plastic strain energy densities.

An example of a typical energy-life curve obtained with JV-approach with the corresponding energy-based properties is shown in figure 2.5.

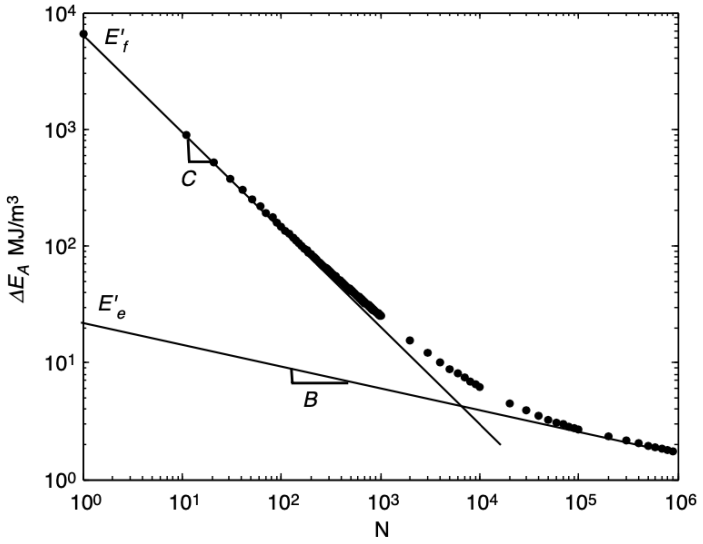

Figure 2.5: Example of a typical energy-life curve obtained using the Jahed-Varvani approach [23].

2.4 Cyclic Hardening / Softening

During constant strain amplitude cyclic loading the stress amplitude can change over the lifetime of a sample. Depending on if the stress is increasing or decreasing, the phenomenon is called cyclic hardening or cyclic softening, respectively. Miner and Castelli [2] investigated the hardening mechanisms in conventional manufactured HX. They observed that HX shows cylic hardening behaviour and they examined the mechanisms contributing to this behaviour. Two main causes for the hardening were found: $M_{23}C_6$ precipitation and increasing dislocation densities.

For additive manufactured HX other cyclic behaviour can be observed due to the different microstructure. According to Esmaeilizadeh [9] LPBF-HX specimens show an increase in the stress amplitude at constant strain amplitudes in the first few cycles of life. Moreover, at higher strain amplitudes the initial hardening is followed by continuous softening. At lower strain amplitudes only slight hardening is observed [9].

2.5 Dynamic Strain Aging

According to Sakthivel et al. [1] Hastelloy X alloy exhibits, as in several Ni-based superalloys and steel, complicated yielding behaviour in the intermediate temperature range. This has been attributed to dynamic strain aging (DSA) phenomenon. Serrated or jerky flow can be observed that occurs after a certain amount of critical plastic strain. The phenomenon can be explained by the dynamic interaction between mobile dislocations with dislocation barriers such as solute atoms [1]. Normally, dislocations are moving during plastic deformation. A cloud of those solute atoms can hold up the dislocations until a certain amount of stress is exceeded. This leads to the serrated flow behaviour.

Chapter 3

Materials and Methods

In this chapter both, the used materials and applied methods are described. After characterizing the properties of the specimen, the experimental setup and testing procedure are explained. Finally, the data analysing methods are described.

3.1 Specimen

The cylindrical specimens used for this project are made of Hastelloy X whose properties are described in section 2.1. They were manufactured by Reza Esmaeilizadeh at University of Waterloo, Canada using a EOS M290 laser powder-bed fusion (LPBF) system. The test samples were fabricated under argon atmosphere with a build plate temperature of 80°C using EOS Hastelloy X powder with a particle size of 15-45 μm [11]. All specimens used for the experiments of this project have the same geometry, shown in figure 3.1.

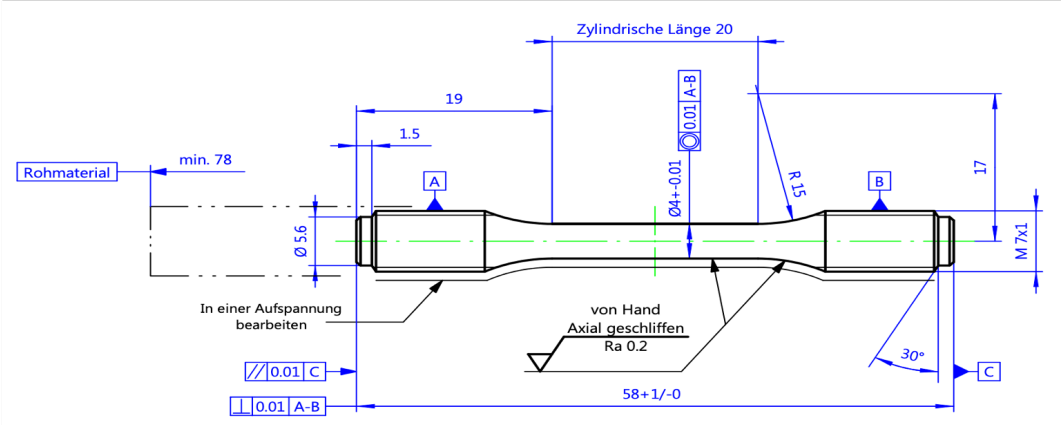

Figure 3.1: Geometry of the specimen used for fatigue tests (dimensions in mm).

In their study [11] Esmaeilizadeh et al. have investigated the effect of LPBF process parameters on static and fatigue behaviour of Hastelloy X. Based on this and previous studies [27] the process parameters listed in table 3.1 were used to produce the samples. The specimens were manufactured vertically, using 67°rotation of the scanning vectors at each successive layer, where the loading direction in mechanical testing was the same as the building direction.

Table 3.1: LPBF process parameters used for printing fatigue specimens [11].

Laser Power [W]	**Laser Scanning Speed** [mm/s]	**Hatching Distance** [mm]	**Layer Thickness** [mm]
195	850	0.09	0.04

As described in section 1.2, one of the objectives of this project is to investigate the influence of the surface roughness on the fatigue response of the material. Therefore, two different specimens were used for comparison. After fabrication in the LPBF-system one version remains unchanged, hereinafter called "as-built". The other version is post-processed to smooth the surface of the specimen, in the following called "surface machined". The two versions used for mechanical fatigue testing are shown in figure 3.2. Finally, threads were added to the ends of all of the specimens in order to clamp them in the testing machine.

Figure 3.2: Comparison of the two versions of the specimen used for mechanical testing. Top: surface machined, bottom: as-built.

3.2 Experimental Setup

Isothermal mechanical experiments were performed using a servo-hydraulic MTS testing machine, as shown in figure 3.3, with a capacity of 100 kN. A

cooper coil is placed around the specimen to heat it up using induction. Three thermocouples (K-type) were used to control and monitor the temperature over the gauge length of the specimen. Normally the thermocouples are spot-welded on the surface of the specimens. Due to the rough surface of the as-built version of the test specimens a proper welding is not possible. Therefore, a ring was formed with the two cables of each thermocouple. The three rings were pulled around the specimen and placed in the centre and at ±5 mm away from the center. The signal of the thermocouple in the center of the specimen was used to control the temperature and keep it at a constant level. As shown in figure 3.3 a side-entry MTS extensometer with a gauge length of 15 mm was used for the measurement and control of the axial strain. To measure the load acting on the test piece an integral load cell was used.

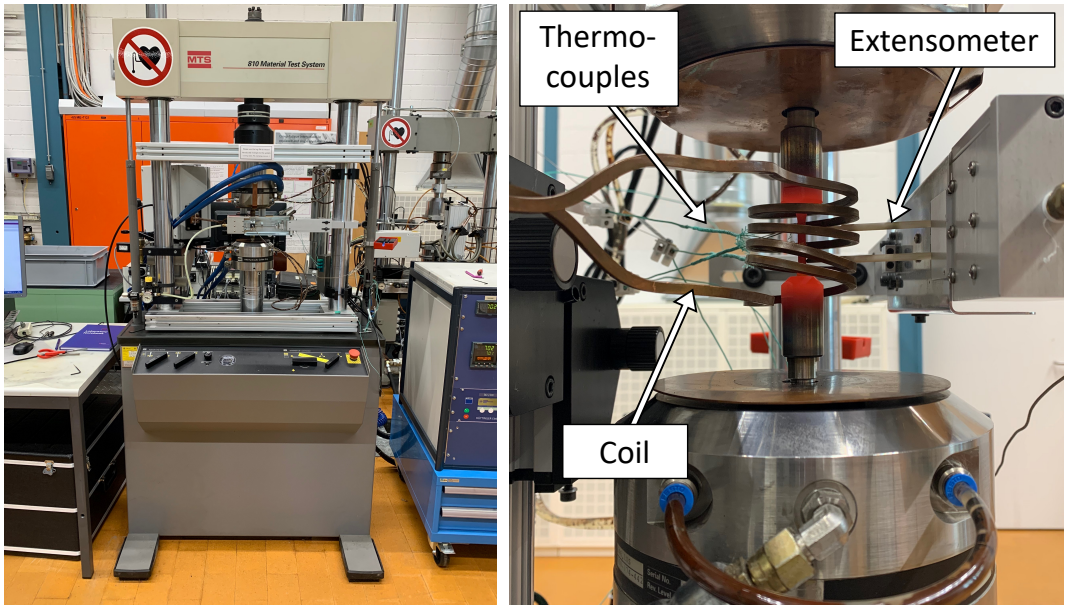

Figure 3.3: a) MTS 100kN testing machine, b) Close up of the fixed and heated specimen.

3.3 Low Cycle Fatigue - Testing

As described in the introduction this project is about the determination of fatigue properties of LBPF Hastelloy X. In this section the procedure of a low-cycle-fatigue (LCF) test according to the International Standard (ISO 12106 [28]) as well as the testing plan of this project is described.

During a test the specimen was uniaxially loaded under strain control at constant amplitude, uniform temperature and strain ratio $R_\varepsilon = -1$. Tests with different strain amplitudes were performed for both surface conditions, all with a constant strain rate of 0.2 $\%s^{-1}$ and at a temperature of 700°C. 17 selected experiments were carried out to characterize the fatigue properties of AM Hastelloy X. If possible, two experiments with the same condition were performed in order to increase the statistical significance of the result. The detailed list of the conducted testing program is listed in table 3.2.

Table 3.2: Summary of test details for the performed LCF-Tests.

Surface machined	**As-built**	**Strain amplitude** [%]	**Number of tests** [#]
x		0.8	2
x		0.5	1
x		0.45	1
x		0.4	2
x		0.3	1
x		0.2	2
x		0.1	1
	x	0.8	2
	x	0.4	2
	x	0.2	2
	x	0.1	1

The fatigue tests were automatically stopped at the cycle the measured stress dropped more than 60% of it's initial value, hereinafter referred to as "total cycles". The number of cycles to failure was defined as the cycle the crack initiation occurs. The procedure to find the number of cycles to failure is decribed in section 3.4.
For each test the following data was recorded and saved:
- E-Modulus at room temperature and at 700°C
- Maximum / Minimum stress of each cycle
- Continuous stress and strain in each cycle
- Temperature of the three thermocouples as a function of time

3.4 Data Analysis

To compare the results from the LCF-Tests three major relationships had to be recorded and plotted:
- Fatigue life (cycle to failure) as a function of strain amplitude
- Maximum / Minimum stress as a function of cycles
- Stress as a function of strain for each cycle (hysteresis loop)

Hysteresis loops of the following cycles were saved for each test: 1, 3, 30, 100, 1000, 3000, etc. including the cycle of crack initiation and the midlife cycle. The midlife cycle is defined as half of the number of cycles to crack initiation.

To find the number of cycles to failure the following procedure, as shown in figure 3.4, was applied after the test was finished: the maximum tensile stress of each cycle was plotted over the number of cycles. To cancel out stress variations at the beginning and at the end only data from the middle third of the cycles was used. For this middle part a linear trend line was fitted at the data points. The criterion for crack initiation was defined as a drop of 5% of the maximum stress. The number of cycles to failure can be read out of the intersection between the maximum stress and the 5% stress-drop function.

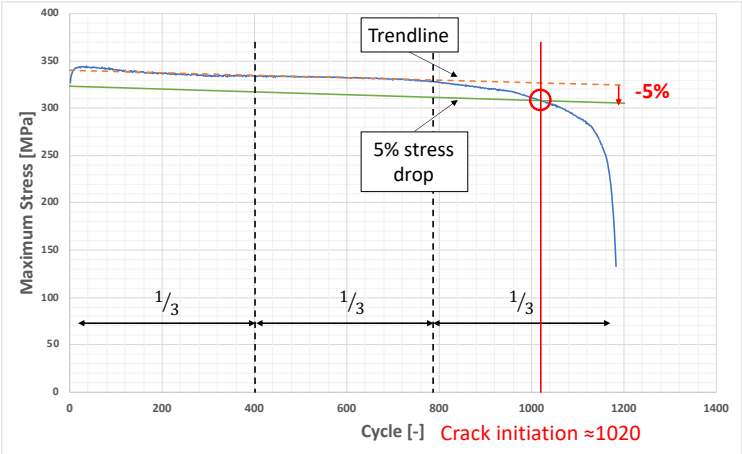

Figure 3.4: Failure criteria: example to find number of cycles to crack initiation.

To extract the needed data out of the generated .txt-files and to determine the number of cycles to failure two Matlab-scripts were developed. The first one assigns the peak and valley stresses to the associated cycle number and calculates the cycle to crack initiation as described above. A second script is used to sort out the data that is needed to generate the hysteresis loops. The codes of the Matlab-scripts are located in the Appendix A - Matlab Scripts.

Chapter 4

Results and Discussion

The following section contains the results of the LCF-Tests and the corresponding interpretation of them. First, some selected hysteresis cycles and peak / valley stresses are shown. After that the implementation of the fatigue life models for one type of tests is done. Finally, the results are compared with data from the literature as described in the objective of this project in section 1.2.

4.1 Fatigue Test Results

4.1.1 Hysteresis - Midlife Cycle

In order to investigate and compare the fatigue behaviour of Hastelloy X 17 LCF-Tests were performed. In this section the stress-strain hysteresis of the midlife cycle of four selected strain amplitudes are shown and compared. The chosen strain amplitudes for the comparison are: 0.8%, 0.4%, 0.2%, and 0.1%. The data from the additional tests was used for the fatigue life calculation. It is necessary to point out that due to problems with the heating-coil and the control loop the deviations between the test temperature and that of the specimens were not always within the 5°C that are specified in the standard for LCF-tests (ISO 12106 [28]).

Figure 4.1 shows the midlife hysteresis of the surface machined condition of two tests per strain amplitude, expect for 0.1%. If a test reached one million cycles it was stopped manually. During the test at 0.1% strain amplitude a problem with oil hydraulic system occurred and the experiment had to be stopped earlier, at 335'000 cycles. For each test the total cycles (end of experiment) and the cycles to failure (crack initiation) are noted. Both tests of the same condition are plotted in the same diagram (blue and orange curve) for a better comparison. In general one can observe that the stress-strain hysteresis for two

tests at equal conditions are quite similar. For some strain amplitudes serrated flow behaviour as described in section 2.5 can be observed, for example it is very pronounced for the strain amplitude of 0.8%. For which conditions the phenomenon occurs and for which it does not, still needs to be investigated in more detail. Another strange observation is the oscillating behaviour in the compression part of the 0.2%-hysteresis. This behaviour is not visible for other strain amplitudes. No inconsistency was found in the data like for example a big temperature gradient fluctuation during the cycle. A possible explanation could be machine noise which results in the undulating shape of the hysteresis. Figure 4.2 shows data of the same strain amplitudes but for the as-built condition. Similar observations can be made as for the previous condition, for example a decreasing stress level for decreasing strain amplitudes. A detailed comparison of the two conditions is described in section 4.2.

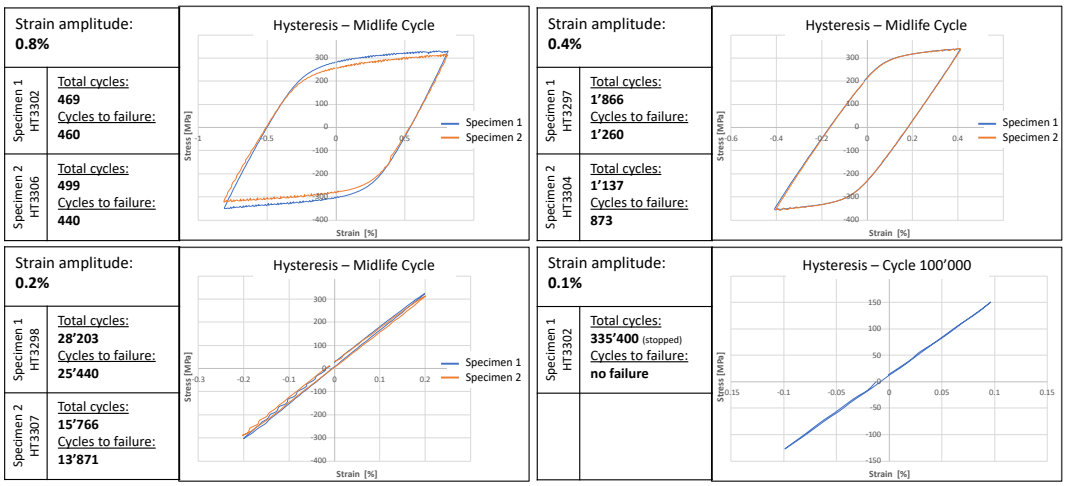

Figure 4.1: Stress-strain hysteresis of the midlife cycle of four selected strain amplitudes: surface machined.

4.1.2 Peak / Valley Stress

Similar to the section above, the results of the four different strain amplitudes are presented in this section. Instead of the hysteresis, the maximum and minimum stress of each cycle are plotted over the cycle number, also referred to as peak / valley stress. Figure 4.3 and Figure 4.4 show the peak / valley stresses of specimens in the surface machined condition and the as-built condition. As before two tests of the same strain amplitude are plotted in one diagram, except for the 0.1% strain amplitude.

It can be seen that a small change of the strain amplitude can have a massive impact on the lifetime of a part. If the curves of two tests with the same

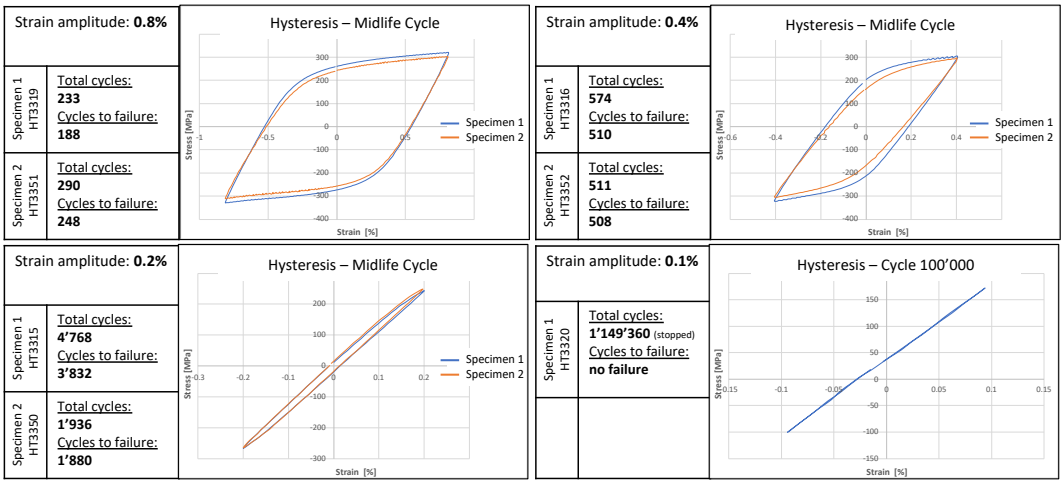

Figure 4.2: Stress-strain hysteresis of the midlife cycle of four selected strain amplitudes: as-built.

conditions are compared, one can observe that most of them show a similar behaviour at the beginning but they can behave quite differently afterwards. In general, two different behaviours are observed: either the course of the curves of the two tests have a similar shape but a different lifetime (e.g. figure 4.3, 0.4%) or they show a different behaviour in the end (e.g. e.g. figure 4.4, 0.2%). An explanation for those big differences in the lifetime could be an existing invisible crack from the inside of a specimen that leads to a much earlier failure. For a better understanding and explanation the fracture surface should be analysed under a microscope to investigate the origin of the crack. The increase of the stress at the end of the orange as-built test at 0.2% (figure 4.2, bottom left) could be explained by a crack that occurred outside of the gauge length of the extensometer. The strange behaviour of the as-built condition at 0.1% could not be explained until now.

Interesting to see is the different cyclic behaviour of the various tests. As described in section 2.4 LCF-deformation of conventional manufactured Hastelloy X at elevated temperature results in continuous cyclic hardening up to failure [29]. Additive manufactured parts show both behaviours, cyclic hardening and cyclic softening. For instance the stress at 0.8% in figure 4.3 decreases (cyclic softening) while it increases for 0.2% strain amplitude (cyclic hardening). Further investigations and more tests have to be done for a better prediction which behaviour is observable at which conditions.

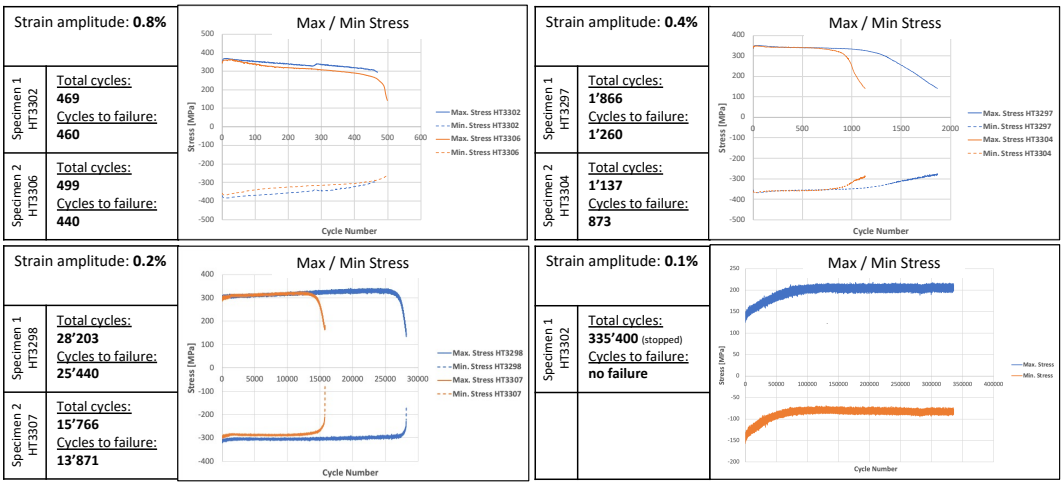

Figure 4.3: Peak / valley stresses of four selected strain amplitudes: surface machined.

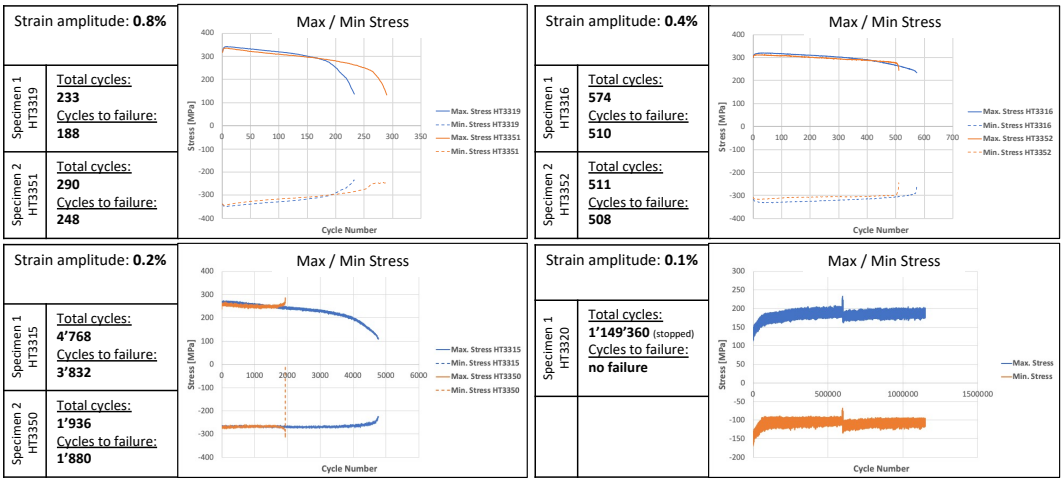

Figure 4.4: Peak / valley stresses of four selected strain amplitudes: as-built.

4.1.3 Fatigue Life Model

In this section the modelling of the fatigue life as described in section 2.3.2 is presented. For the fatigue life prediction the results of the 0.1% strain amplitude tests have not been taken into account since they had to be stopped and therefore did not fail. The parameters of Basquin-Coffin-Manson model and the Jahed-Varvani model are calculated and listed in table 4.1 and 4.2, respectively.

The parameters are used in Eq. 2.3 and Eq. 2.6 to calculate the BCM strain-life curve and the JV energy-life curve, respectively. For the surface machined

Table 4.1: BCM fatigue life model parameters for HX.

	$\frac{\sigma_f^{'}}{E}$	$\varepsilon_f^{'}$	b	c
Surface machined	1.0567	2057.9	-0.097	-1.131
As-built	1.511	6597.5	-0.162	-1.449

Table 4.2: JV fatigue life model parameters for HX.

	$E_e^{'}$	$E_f^{'}$	B	C
Surface machined	0.4924	23672	-0.036	-1.215
As-built	1.1325	7522.7	-0.187	-1.561

condition the predicted life-curves of the two approaches including experimental points are shown in figure 4.5. In the same graphs the functions of the elastic/plastic strain and elastic/plastic energy density are plotted.

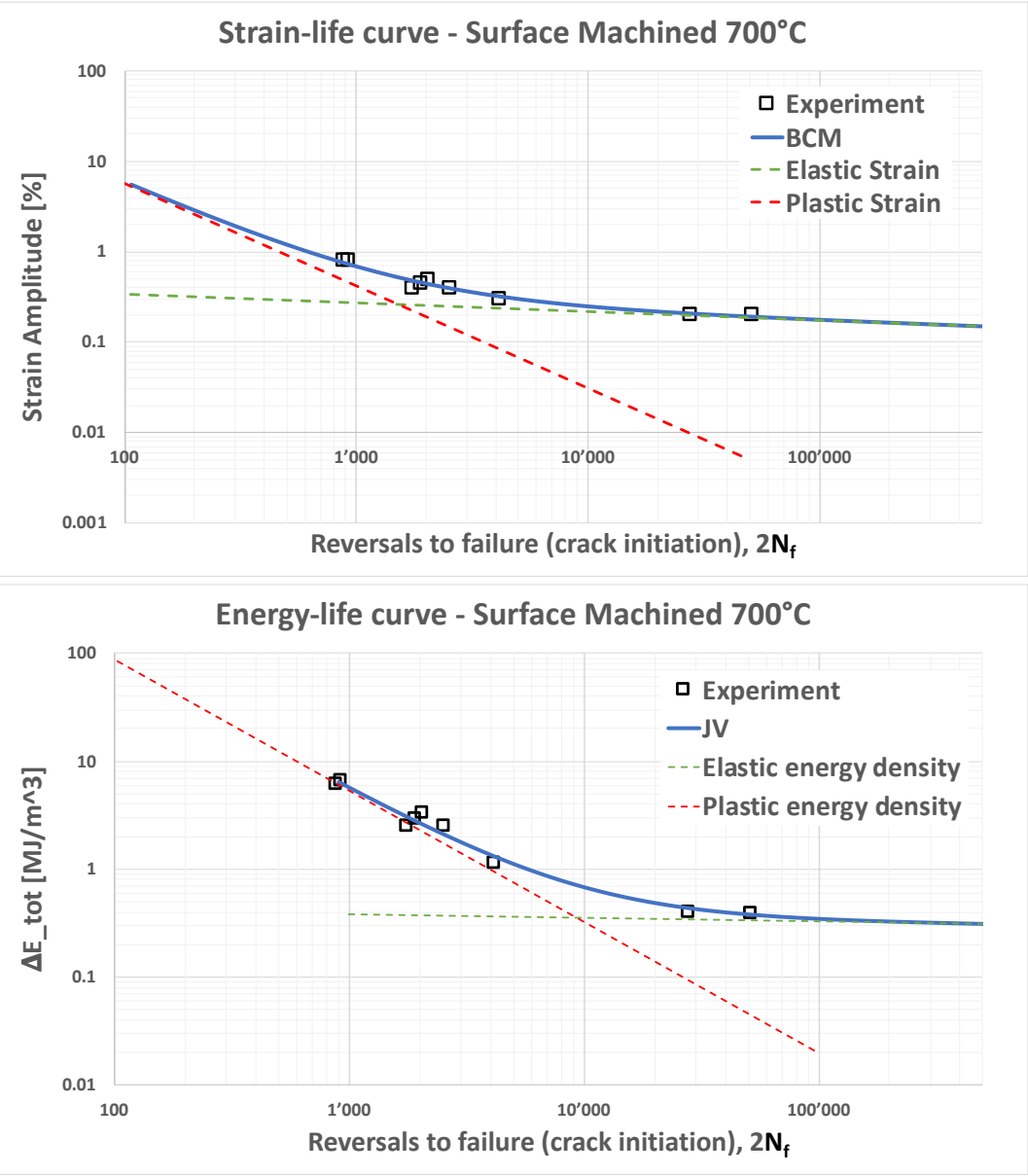

Figure 4.5: Top: modelled strain-life curve of the surface machined condition using BCM-approach, Bottom: modelled energy-life curve of the surface machined condition using JV-approach.

4.2 Comparison: As-built vs. Surface machined

In the following the fatigue behaviour of the two investigated conditions, surface machined and as-built, is compared. For illustration two strain amplitudes are selected: 0.8% and 0.2%. Figure 4.6 shows a comparison of the midlife hysteresis and the peak / valley stresses for both conditions at the two strain

amplitudes. The blue curves belong to the surface machined specimens while the orange curves show the behaviour of the as-built condition. In general it can be said that the stress level is lower for the as-built condition. This can be due to smaller actual cross section. As mentioned before different cyclic behaviour is shown for different conditions. As it can be seen in figure 4.6 the surface machined condition shows a cyclic hardening at 0.2% strain amplitude while the as-built condition shows cyclic softening.

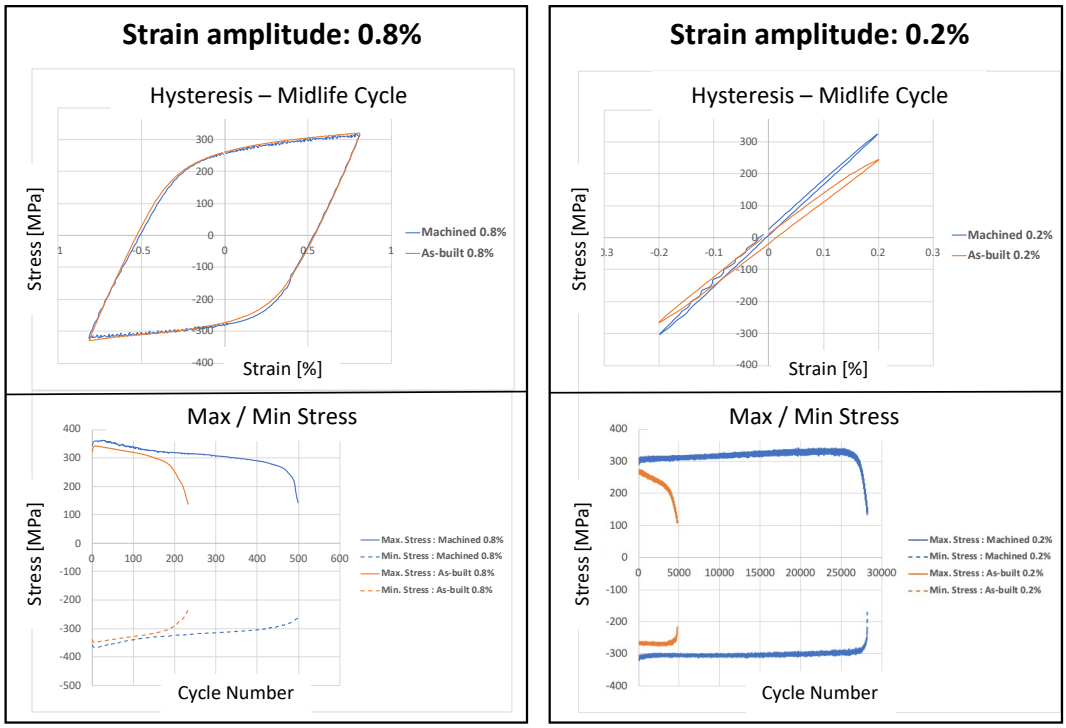

Figure 4.6: Comparison of surface machined and as-built condition at 0.2% and 0.8% strain amplitude.

Interesting to compare is the average of the lifetime of the two conditions. In table 4.3 the average cycles to failure of three different strain amplitudes (0.8%, 0.4%, 0.2%) are listed. It can be seen that with decreasing strain amplitude the difference of the lifetime increases. This observation can be explained by investigation of the crack initiation and growth. With a small strain amplitude, for example 0.2%, it takes a lot of time to create the first crack at the surface. Due to the rough surface of the as-built condition there exist already many "sources" for a crack initiation. Therefore a crack can occur much earlier compared to a surface machined part despite of the small strain amplitude. The higher the strain amplitude, the smaller the effect of the surface roughness takes into account and therefore the difference between the cycles to failure tends to be smaller.

Table 4.3: Comparison of fatigue-life: surface machined vs. as-built.

Strain amplitude	Failure cycles: Machined	Failure cycles: As-built	percent change
0.8	450	218	-52 %
0.4	1067	509	-52 %
0.2	19656	2856	-82 %

4.3 Comparison: Room Temperature vs. 700°C

Next, the obtained results are compared to the results from Esmaeilizadeh [9] that have been done under the same conditions at room temperature. The room temperature tests have been done with specimens at the "as-built" condition. For comparison at 700°C both, as-built and surface machined condition, are used. Strain-life curves of the three conditions described above, modelled with the BCM-approach, are plotted in figure 4.7. Notice: for the reversals to failure at room temperature it is not clear, how "failure" was defined for the tests.
As excepted the material shows a lower fatigue life at higher temperatures. For the machined condition the fatigue life decreases by a factor of about 2-10, for the as-built condition about 5-30. Due to the fact, that the experiments at 700°C for 0.1% strain amplitude were stopped manually, there exist no data points for failure at this amplitude. For a better comparison data at lower strain amplitudes (0.1% and 0.07%) for 700°C would be necessary.

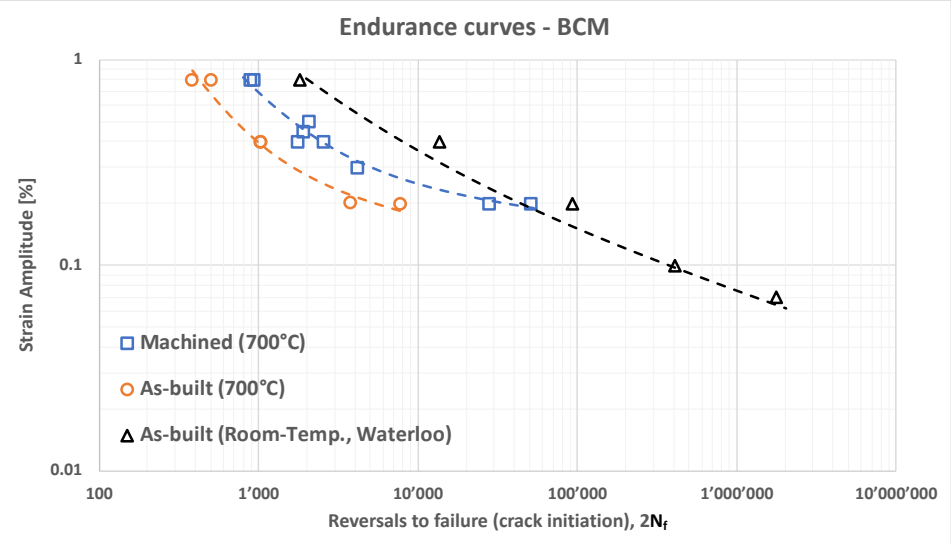

Figure 4.7: Comparison of BCM strain-life curves at room temperature and at 700°C.

4.4 Comparison: Additive Manufactured vs. Conventional Manufactured

As a last comparison the results from the tests are compared to data for conventional manufactured Hastelloy X. Brinkman et al. [30] performed fatigue tests on conventional manufactured HX at 649°C and at 760°C. It's not the same temperature as used for the AM-tests, but it's sufficient for a comparison.

Figure 4.8 shows the strain-life curves of four different test conditions: as-built and surface machined HX at 700°C and conventional manufactured HX at 649°C and 760°C. The fatigue life curves are modelled using the BCM-approach. It can be clearly seen that the fatigue life of AM HX is shorter than for conventional manufactured. This can be explained by the porosities and rough surfaces of the AM-parts that promote the formation of cracks. One can also observe that the difference in the lifetime between AM and conventional increases for smaller strain amplitudes. AM-parts generally have a higher yield strength and therefore a higher fatigue strength. For small strain amplitudes the deformation plays a subordinate role with regard to crack formation. Rather, the defects of AM materials are most likely responsible for crack initiation and growth. Therefore the lifetime is even shorter at small strains. For higher strain amplitudes the effect of the defects is less distinctive and therefore the expected lifetimes are closer together.

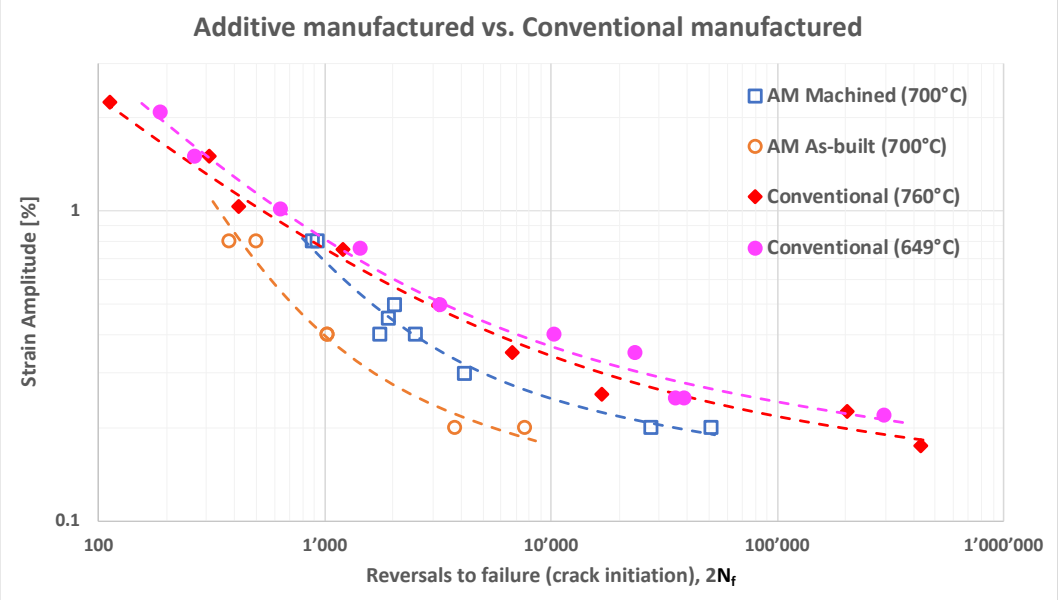

Figure 4.8: Comparison of BCM strain-life curves of additive and conventional manufactured HX.

Chapter 5

Conclusion

Fatigue tests of Hastelloy X at 700°C were performed. The effect of surface roughness was investigated by using two different surface conditions. To model the fatigue life two different approaches, Basquin-Coffin-Manson and Jahed-Varani, were used. The data of the fatigue tests was evaluated and the results were then compared with data from the literature. In summary, three different comparisons were made: room temperature LPBF-HX vs. LPBF-HX at 700°C, additive manufactured HX vs. conventional manufactured HX and as-built vs. surface machined HX.

With the results from the fatigue tests together with data from the literature the following observations and conclusions can be made:

- The stress-strain hysteresis shows serrated flow behaviour at some conditions, but not always.
- Two tests at the same test conditions can show a big difference in the lifetime, among other things because of internal defects.
- AM Hastelloy X can show both, cyclic hardening or cyclic softening.
- Both fatigue life approaches can be applied to the fatigue life data, each with its own advantages and disadvantages.
- The lifetime of additive manufactured parts out of Hastelloy X is shorter than for conventional manufactured.
- The surface roughness can have a big influence on the fatigue life and the fatigue behaviour of a part. The expected fatigue life for as-built parts can decrease by up to 85% compared to surface machined parts.
- More scatter is observed for the surface machined condition than for the as-built condition. An explanation for the observation could be, that

as-built parts have many options for a crack initiation due to the rough surface. Therefore all specimens have the same "initial" condition and the crack initiation occurs approximately at the same amount of cycles. The surface machined specimens have all the same, smooth surface. But one specimen could have an internal defect and another one not. The lifetime is dependent on these defects and therefore more scatter in the results is observable.

- Depending on the amplitude, the lifetime of a part at 700°C can decrease by a factor of 5-30 compared to the same conditions at room temperature.
- AM Hastelloy X fails earlier compared to conventional manufactured. The difference between the cycles to failure increases with decreasing strain amplitudes.

5.1 Outlook

In the future, the investigation of the fatigue behaviour of LPBF-Hastelloy X at high temperatures should be continued. Due to the scope of the project only one or two tests per strain amplitude have been performed. The more data available, the better some phenomenons and observations can be explained and the more the statistical significance is increased. Therefore, more experiments at more different strain amplitudes and possibly different temperatures should be done. The test procedure could still be improved to provide more constant and less error-prone results. Especially the induction heating could be improve in order to ensure a constant and isothermal temperature distribution and to always achieve the targets from the standard.

For some tests the fatigue behaviour could only be described but not always explained. Some inconsistencies and strange behaviours, like unexplainable peaks, should be examined again more closely. Another possibility would be to have a look at the fracture surface under a SEM (scanning electron microscope) in order to investigate the crack initiation and growth.

List of Figures

List of Tables

Bibliography

[1] T Sakthivel, K Laha, M Nandagopal, KS Chandravathi, P Parameswaran, S Panneer Selvi, MD Mathew, and Sarwan K Mannan. Effect of temperature and strain rate on serrated flow behaviour of hastelloy x. *Materials Science and Engineering: A*, 534:580–587, 2012.

[2] RV Miner and MG Castelli. Hardening mechanisms in a dynamic strain aging alloy, hastelloy x, during isothermal and thermomechanical cyclic deformation. *Metallurgical Transactions A*, 23(2):551–561, 1992.

[3] HU Hong, IS Kim, BG Choi, HW Jeong, and CY Jo. Effects of temperature and strain range on fatigue cracking behavior in hastelloy x. *Materials Letters*, 62(28):4351–4353, 2008.

[4] Vojislav Petrovic, Juan Vicente Haro Gonzalez, Olga Jordá Ferrando, Javier Delgado Gordillo, Jose Ramón Blasco Puchades, and Luis Portolés Griñan. Additive layered manufacturing: sectors of industrial application shown through case studies. *International Journal of Production Research*, 49(4):1061–1079, 2011.

[5] Wei Gao, Yunbo Zhang, Devarajan Ramanujan, Karthik Ramani, Yong Chen, Christopher B Williams, Charlie CL Wang, Yung C Shin, Song Zhang, and Pablo D Zavattieri. The status, challenges, and future of additive manufacturing in engineering. *Computer-Aided Design*, 69:65–89, 2015.

[6] Liubov Magerramova, Boris Vasilyev, and Vladimir Kinzburskiy. Novel designs of turbine blades for additive manufacturing. In *ASME Turbo Expo 2016: Turbomachinery Technical Conference and Exposition*. American Society of Mechanical Engineers Digital Collection, 2016.

[7] Behzad Fotovvati, Navid Namdari, and Amir Dehghanghadikolaei. Fatigue performance of selective laser melted ti6al4v components: state of the art. *Materials research express*, 6(1):012002, 2018.

[8] Anton du Plessis, Ina Yadroitsava, and Igor Yadroitsev. Effects of defects on mechanical properties in metal additive manufacturing: A review focusing on x-ray tomography insights. *Materials & Design*, 187:108385, 2020.

[9] Reza Esmaeilizadeh. Characterization and modelling of additively manufactured hastelloy x parts under quasi-static and cyclic loading. 2021.

[10] Fude Wang. Mechanical property study on rapid additive layer manufacture hastelloy® x alloy by selective laser melting technology. *The International Journal of Advanced Manufacturing Technology*, 58(5-8):545–551, 2012.

[11] Reza Esmaeilizadeh, Ali Keshavarzkermani, Usman Ali, Behzad Behravesh, Ali Bonakdar, Hamid Jahed, and Ehsan Toyserkani. On the effect of laser powder-bed fusion process parameters on quasi-static and fatigue behaviour of hastelloy x: A microstructure/defect interaction study. *Additive Manufacturing*, 38:101805, 2021.

[12] Jonas Saarimäki, Mattias Lundberg, Håkan Brodin, and Johan J Moverare. Dwell-fatigue crack propagation in additive manufactured hastelloy x. *Materials Science and Engineering: A*, 722:30–36, 2018.

[13] Bo Song, Daniel Casem, and Jamie Kimberley. *Dynamic Behavior of Materials, Volume 1*. Springer, 2012.

[14] Richard Leach and Simone Carmignato. *Precision Metal Additive Manufacturing*. CRC Press, 2020.

[15] Li Yang, Keng Hsu, Brian Baughman, Donald Godfrey, Francisco Medina, Mamballykalathil Menon, and Soeren Wiener. *Additive manufacturing of metals: the technology, materials, design and production*. Springer, 2017.

[16] John O Milewski. Additive manufacturing of metals. *Applied Mechanics and Materials*, 2017.

[17] W Meiners, S Bremen, and A Diatlov. Selective laser melting–additive manufacturing for series production of the future? In *INTERMAT 2011 on Rapid Manufacturing Conference, Luxembourg, 1st Feb*, 2011.

[18] Almar A Naess. *Fatigue handbook: offshore steel structures*. Tapir, 1985.

[19] Weicheng Cui. A state-of-the-art review on fatigue life prediction methods for metal structures. *Journal of marine science and technology*, 7(1):43–56, 2002.

[20] Jaap Schijve. *Fatigue of structures and materials*. Springer Science & Business Media, 2001.

[21] Johannes Dallmeier, Otto Huber, Holger Saage, Klaus Eigenfeld, and Andreas Hilbig. Quasi-static and fatigue behavior of extruded me21 and twin roll cast az31 magnesium sheet metals. *Materials Science and Engineering: A*, 590:44–53, 2014.

[22] S Begum, DL Chen, S Xu, and Alan A Luo. Low cycle fatigue properties of an extruded az31 magnesium alloy. *International Journal of Fatigue*, 31(4):726–735, 2009.

[23] H Jahed and A Varvani-Farahani. Upper and lower fatigue life limits model using energy-based fatigue properties. *International Journal of Fatigue*, 28(5-6):467–473, 2006.

[24] SMH Karparvarfard, Sugrib K Shaha, Seyed Behzad Behravesh, Hamid Jahed, and Bruce W Williams. Fatigue characteristics and modeling of cast and cast-forged zk60 magnesium alloy. *International Journal of Fatigue*, 118:282–297, 2019.

[25] ASTM Standard. E739-10, standard practice for statistical analysis of linear or linearized stress-life (sn) and strain-life (ε-n) fatigue data. *Annual Book of ASTM Standards, American Society for Testing and Materials, West Conshohocken, PA*, 3:721–727, 2012.

[26] H Jahed and J Albinmousa. Multiaxial behaviour of wrought magnesium alloys–a review and suitability of energy-based fatigue life model. *Theoretical and Applied Fracture Mechanics*, 73:97–108, 2014.

[27] Reza Esmaeilizadeh, Ali Keshavarzkermani, Usman Ali, Yahya Mahmoodkhani, Behzad Behravesh, Hamid Jahed, Ali Bonakdar, and Ehsan Toyserkani. Customizing mechanical properties of additively manufactured hastelloy x parts by adjusting laser scanning speed. *Journal of Alloys and Compounds*, 812:152097, 2020.

[28] ISO 12106: 2017. Metallic materials-fatigue testing-axial-strain-controlled method, 2017.

[29] GV Prasad Reddy, P Harini, R Sandhya, K Bhanu Sankara Rao, and RK Paretkar. On dual-slope linear cyclic hardening of hastelloy x. *Materials Science and Engineering: A*, 527(16-17):3848–3851, 2010.

[30] CR Brinkman, PL Rittenhouse, WR Corwin, JP Strizak, Aage Lystrup, and JR DiStefano. Application of hastelloy x in gas-cooled reactor systems. Technical report, Oak Ridge National Lab., Tenn.(USA), 1976.

Appendices

Appendix A - Matlab Scripts

Extract data from selected cycles:

```
clear
clc
close all
TestNumber = 1;
set(0,'DefaultAxesFontSize', 14)
Originalpath=cd;
[spec_ID,path] = uigetfile('*.txt','select data record');
cd(path);
fid = fopen(spec_ID);
data = textscan(fid,'%f %f %f %f %f %f %f %f %f %f','Headerlines',8,'delimiter','whitespace');
fclose(fid);
addpath (Originalpath)

prompt = {'Enter HT number:'};
dims = [1 35];
dlgtitle = 'Input';
HT_number = inputdlg(prompt,dlgtitle,dims);

prompt = {'Enter cycles to crack initiation:'};
dims = [1 35];
dlgtitle = 'Input';
crack_initiation = inputdlg(prompt,dlgtitle,dims);

cyc_crackini    = str2double(crack_initiation);


% Generation of stress and strain data vectors
Stress = zeros(length(data{1,1}),1);
Strain_tot = zeros(length(data{1,1}),1);
Time = zeros(length(data{1,1}),1);
T_mid = zeros(length(data{1,1}),1);
T_top = zeros(length(data{1,1}),1);
T_bot = zeros(length(data{1,1}),1);


%cycle 1
cyc_second_column   = find(data{1,2}==2, 1, 'last');
cyc1_start          = find(data{1,1}==1, 1, 'first');
cyc1_end            = cyc_second_column;
cyc1_time           = data{1,3}(cyc1_start:cyc1_end)-data{1,3}(cyc1_start);
cyc1_strain         = data{1,4}(cyc1_start:cyc1_end)*100;
cyc1_stress         = data{1,5}(cyc1_start:cyc1_end)*1e3;
cyc1_temp_mid       = data{1,6}(cyc1_start:cyc1_end);
cyc1_temp_top       = data{1,8}(cyc1_start:cyc1_end);
cyc1_temp_bot       = data{1,9}(cyc1_start:cyc1_end);
```

Repeat for cycles 3, 10, 30, 300, etc.

Extract the needed data and calculate the cycle of crack initiation:

```
clear
clc
close all
TestNumber = 1;
set(0,'DefaultAxesFontSize', 14)
Originalpath=cd;
[spec_ID,path] = uigetfile('*.txt','select data record');
cd(path);
fid = fopen(spec_ID);
data = textscan(fid,'%f %f %f %f %f %f %f %f %f %f','Headerlines',8,'delimiter','whitespace');
fclose(fid);
addpath (Originalpath)

prompt = {'Enter HT number:'};
dims = [1 35];
dlgtitle = 'Input';
HT_number = inputdlg(prompt,dlgtitle,dims);

% Generation of stress and strain data vectors
Stress = zeros(length(data{1,1}),1);
Strain_tot = zeros(length(data{1,1}),1);
Time = zeros(length(data{1,1}),1);
T_mid = zeros(length(data{1,1}),1);
T_top = zeros(length(data{1,1}),1);
T_bot = zeros(length(data{1,1}),1);

ind=find(data{1,1}==1, 1, 'first');
cyc         = data{1,1}(ind:end);
cyc_odd     = cyc(1:2:end);
Stress      = data{1,5}(ind:end)*1e3;
Stress_max  = Stress(1:2:end);
Stress_min  = Stress(2:2:end);
%Strain_tot  = data{1,4}(ind:end)*100;
%Time        = data{1,3}(ind:end)-data{1,2}(1);
%T_mid       = data{1,6}(ind:end);
%T_top       = data{1,8}(ind:end);
%T_bot       = data{1,9}(ind:end);

writematrix(cyc_odd,'peak_valley_copy.xlsx','Sheet',1,'Range','A2');
writematrix(Stress_max,'peak_valley_copy.xlsx','Sheet',1,'Range','B2');
writematrix(Stress_min,'peak_valley_copy.xlsx','Sheet',1,'Range','C2');
writecell(HT_number,'peak_valley_copy.xlsx','Sheet',1,'Range','F1');
```

```
% function to calculate the 5%-force drop: (copied)

% 'ncycles' designates the number of full cycles recorded in a certain test
ncycles = length(cyc_odd);
start_fit = floor((1/3)*ncycles);
end_fit = ceil((2/3)*ncycles);

% Linear fit to the data (maximal stress vs. cycle number) between
% 1/3 and 2/3 of ncycles
linear_fit_cyc = cyc_odd(start_fit:1:end_fit);
linear_fit_stress = Stress_max(start_fit:1:end_fit);
coeffs_nominal = polyfit(linear_fit_cyc,linear_fit_stress,1);

% Construction of a straight line with the same slope as the linear fit
% derived above but with values that are 5% with respect to stress lower
% throughout
coeffs_drop(1) = coeffs_nominal(1);
coeffs_drop(2) = (0.95)*coeffs_nominal(2);

coeffs_stress_max = polyfit(cyc_odd,Stress_max,5);

diff = polyval(coeffs_stress_max,cyc_odd)-polyval(coeffs_drop,cyc_odd);

% If 'diff' becomes negative, the cycle with a 5% low drop with respect to
% stress 'N_5percent' has been found
% '+1' in order to minimize conservativity
N_5percent = cyc_odd(1+find(diff>0,1,'last'));

writematrix(N_5percent,'peak_valley_copy.xlsx','Sheet',1,'Range','J1');

```

Eidgenössische Technische Hochschule Zürich
Swiss Federal Institute of Technology Zurich

Eigenständigkeitserklärung

Die unterzeichnete Eigenständigkeitserklärung ist Bestandteil jeder während des Studiums verfassten Semester-, Bachelor- und Master-Arbeit oder anderen Abschlussarbeit (auch der jeweils elektronischen Version).

Die Dozentinnen und Dozenten können auch für andere bei ihnen verfasste schriftliche Arbeiten eine Eigenständigkeitserklärung verlangen.

Ich bestätige, die vorliegende Arbeit selbständig und in eigenen Worten verfasst zu haben. Davon ausgenommen sind sprachliche und inhaltliche Korrekturvorschläge durch die Betreuer und Betreuerinnen der Arbeit.

Titel der Arbeit (in Druckschrift):

Cyclic plasticity and fatigue response of SLM Hastelloy X at 700

Verfasst von (in Druckschrift):
Bei Gruppenarbeiten sind die Namen aller Verfasserinnen und Verfasser erforderlich.

Name(n):	**Vorname(n):**
Kuhlow	Mathias

Ich bestätige mit meiner Unterschrift:
- Ich habe keine im Merkblatt „Zitier-Knigge" beschriebene Form des Plagiats begangen.
- Ich habe alle Methoden, Daten und Arbeitsabläufe wahrheitsgetreu dokumentiert.
- Ich habe keine Daten manipuliert.
- Ich habe alle Personen erwähnt, welche die Arbeit wesentlich unterstützt haben.

Ich nehme zur Kenntnis, dass die Arbeit mit elektronischen Hilfsmitteln auf Plagiate überprüft werden kann.

Ort, Datum	**Unterschrift(en)**
Weinfelden, 18. Juni 2021	M. Kuhlow

Bei Gruppenarbeiten sind die Namen aller Verfasserinnen und Verfasser erforderlich. Durch die Unterschriften bürgen sie gemeinsam für den gesamten Inhalt dieser schriftlichen Arbeit.